CHEMISTRY
A EUROPEAN JOURNAL

DOI: 10.1002/chem.200701717

Thiophene Polymer Semiconductors for Organic Thin-Film Transistors

Beng S. Ong,*[a] Yiliang Wu,[b] Yuning Li,[b] Ping Liu,[b] and Hualong Pan[b]

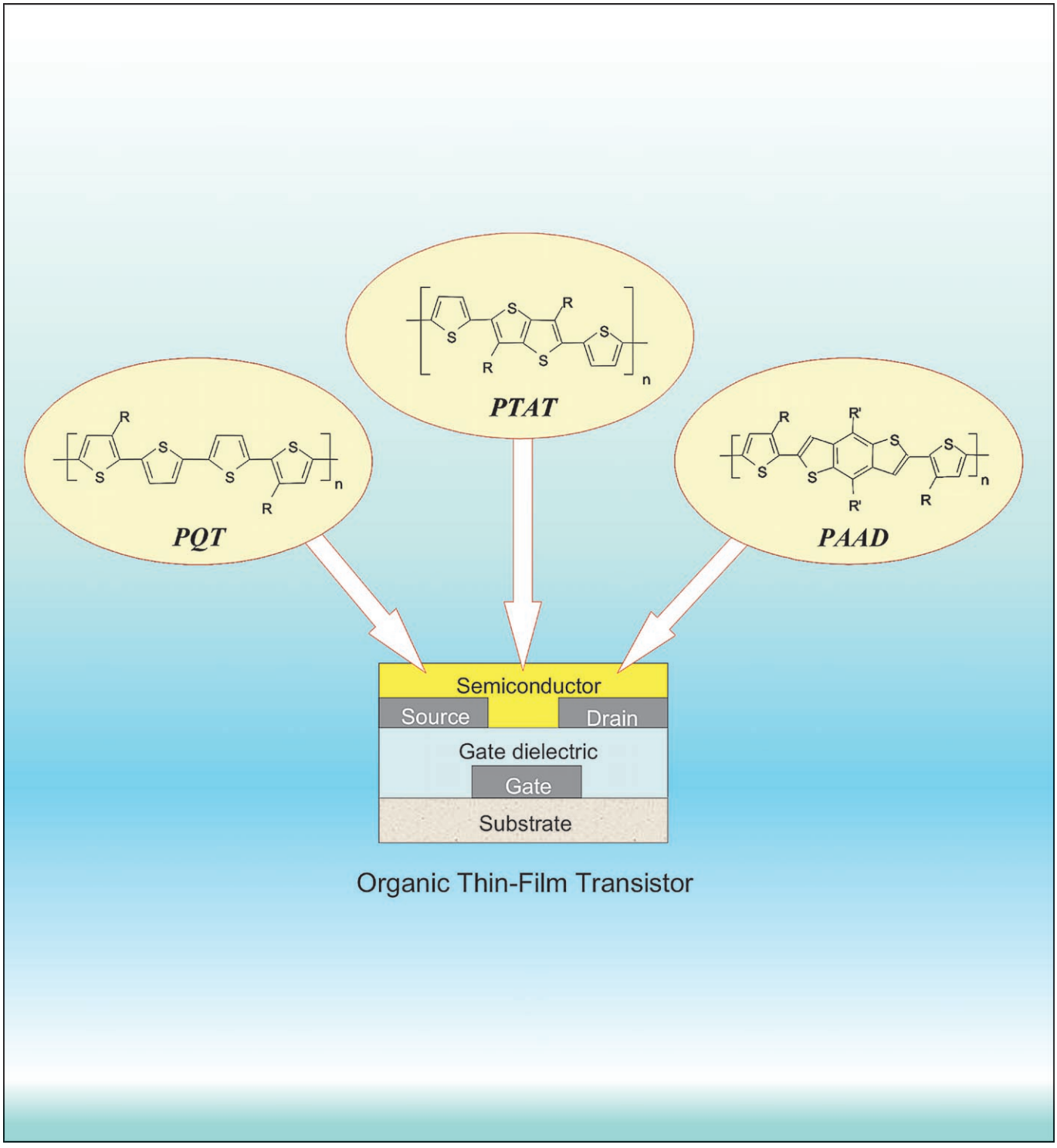

Abstract: Printed organic thin-film transistors (OTFTs) have received great interests as potentially low-cost alternative to silicon technology for application in large-area, flexible, and ultra-low-cost electronics. One of the critical materials for TFTs is semiconductor, which has a dominant impact on the transistor properties. We review here the structural studies and design of thiophene-based polymer semiconductors with respect to solution processability, ambient stability, molecular self-organization, and field-effect transistor properties for OTFT applications. We show that through judicial monomer design, delicately controlled π-conjugation, and strategically positioned pendant side-chain distribution, novel solution-processable thiophene polymer semiconductors with excellent self-organization ability to form extended lamellar π-stacking orders can be developed. OTFTs using semiconductors of this nature processed in ambient conditions have provided excellent field-effect transistor properties.

Keywords: field-effect transistors · printed electronics · semiconductors · thin films · thiophenes

Introduction

Organic thin-film transistors have received profound interest in recent years for their potential as a low-cost alternative to amorphous hydrogenated silicon thin-film transistors for various electronic applications.[1] OTFT-based arrays/circuits are particularly suited for large-area devices (e.g., active-matrix displays) where high transistor density and switching speeds are not essential;[2] they may also be attractive for applications in low-end microelectronics (e.g., radio frequency identification tags, sensors, etc.) where the high cost of packaging silicon circuits becomes a prohibitive factor to ubiquitous usage.[1] The economic advantage of OTFTs stems from significantly lower-cost manufacturing capital investments as well as low-cost fabrication using common solution-based deposition and patterning techniques (e.g., offset, gravure, screen/stencil printing, inkjet printing, etc.).[3] Such OTFT arrays/circuits, particularly those based on polymers, can also be fabricated on plastic substrates so that compact, lightweight, and structurally robust and flexible electronic devices (e.g., e-paper) can be constructed.

Figure 1 shows a schematic depiction of OTFTs in three common configurations. An OTFT is comprised of three electrodes (source, drain and gate), a gate dielectric layer, and an organic or polymer semiconductor layer. In operation, an electric field is applied across the source-drain electrodes, and the transistor is turned on when a voltage (V_G) is applied to the gate electrode, which induces a current flow (I_D) from the source electrode to drain electrode. When $V_G = 0$, the transistor is turned off, I_D should in theory be 0, that is, no current flowing through. This is to say that

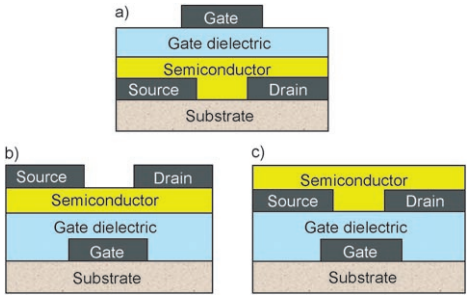

Figure 1. Schematic structures of TFTs: a) top-gate, top-contact; b) bottom-gate, top-contact; c) bottom-gate, bottom-contact.

at a constant source-drain electric field, I_D is modulated by V_G. The transistor performance is generally characterized by the current-voltage plots, that is, output (Figure 2a) and transfer (Figure 2b) curves, where critical parameters such as field-effect transistor (FET) mobility (μ), current on/off ratio (I_{on}/I_{off}), threshold voltage (V_T), subthreshold swing can be extracted. If the current/voltage characteristics follow closely the metal oxide-semiconductor field-effect transistor (FET) gradual channel model, μ can be extracted from the standard MOSFET equations:

$$\text{linear regime } (V_D \ll V_G): I_D = V_{SD} C_i \mu (V_G - V_T)(W/L)$$

$$\text{saturated regime } (V_D > V_G): I_D = C_i \mu (W/2L)(V_G - V_T)^2$$

where V_{SD} is the drain voltage with the source electrode being grounded. W and L are the transistor channel width and length, respectively, and C_i is the capacitance per unit area of the dielectric layer.

A bottom-gate, top-contact (Figure 1b) or a bottom-gate, bottom-contact (Figure 1c) TFT test structure was used to evaluate the FET performance of our semiconductors. The experimental OTFT devices are built on an n-doped silicon wafer (gate electrode) with a 100 or 200 nm thermal silicon

[a] Prof. Dr. B. S. Ong
Institute of Materials Research & Engineering (IMRE)
Agency of Science, Technology and Research (A*STAR)
3 Research Link, Singapore 117602
Fax: (+65) 6874-8111
E-mail: ongb@imre.a-star.edu.sg
bengong@ntu.edu.sg
and
School of Materials Science & Engineering, Nanyang Technological University, Singapore 639798

[b] Dr. Y. Wu, Dr. Y. Li, P. Liu, Dr. H. Pan
Materials Design & Integration Laboratory
Xerox Research Centre of Canada
Mississauga, ON L5K 2L1 (Canada)

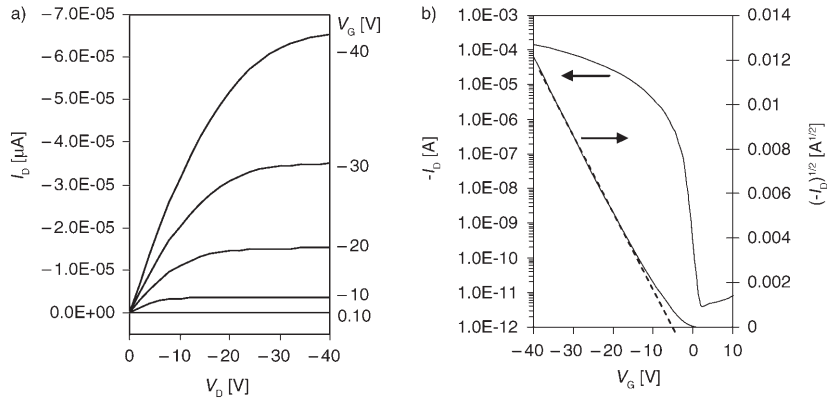

Figure 2. Illustrative current-voltage curves of a thin-film transistor: (a) output curve showing source/drain current as a function of source/drain voltage at constant gate voltage; and (b) transfer curve showing source/drain current as a function of gate voltage at constant source/drain voltage [Ref. 41].

oxide (SiO_2) dielectric layer, which was modified with a self-assembled monolayer of octyltrichlorosilane (OTS-8) to promote molecular ordering in the semiconductor layer. For the top-contact device, the semiconductor layer ($\approx$20–50 nm) was deposited on the OTS-8-modified SiO_2 surface by spin coating. A series of gold source-drain electrode pairs were subsequently deposited on top of the semiconductor layer by vacuum evaporation through a shadow mask, thus forming an array of OTFTs with various channel length and width dimensions. For the bottom-contact device, semiconductor polymer was spin coated after gold electrode deposition. The commonly reported FET mobility, μ and current on/off ratio, I_{on}/I_{off} are respectively charge carrier velocity per unit electric field and ratio of on-current over off-current. For many useful applications, μ is required to be $\geq 0.1\ cm^2 V^{-1} s^{-1}$ while $I_{on}/I_{off} \geq 10^4$. Ideally desirable TFTs will have a V_T close to zero.

One of the critical materials, which have a dominant influence on the FET performance of OTFTs, are semiconductors. There are three basic types of semiconductor materials depending on their ability to conduct holes (p-type), electrons (n-type) or both (ambipolar) under different gate bias conditions. Until relatively recently, organic semiconductors for TFTs were particularly challenging to work with as most of them were either insoluble or very sensitive to air under ambient conditions. Insoluble materials preclude the use of solution deposition while air sensitivity requires manufacturing in an inert atmosphere; both of these restrictive requirements invariably lead to increased cost, thereby nullifying the fundamental economic advantage of OTFTs. Some small molecular semiconductors exhibit high FET mobility when deposited by vacuum evaporation, but their performance deteriorate drastically when solution cast—a generally phenomenon attributed to poor film quality and/or difficulty in establishing continuous, ordered molecular layers at the dielectric interface from solution deposition. Polymer semiconductors generally display lower mobility, but their easy solution processability and good film-forming property offer excellent opportunities for use in fabricating low-cost OTFTs. Among p-type polymer semiconductors such as polytriarylamines,[4] polyindolo-carbazoles,[5] thiophene-based polymers have been shown to be the most promising semiconductor candidates for OTFTs.[6] This article focuses on the development of thiophene polymer semiconductors and our progress in the design of high-performance thiophene polymer semiconductors for solution-processed OTFT applications.

Polymer Semiconductors: Issues, Challenges

While FET properties in organic materials were first observed in the 1960s,[7] little progress were made until two decades later when several organic semiconductors were demonstrated in OTFTs.[8–10] Since then great strides have been made, with the current mobility not only rivals but supersedes those of amorphous hydrogenated silicon.[11,12] Nonetheless, the high mobility was mostly obtained from vacuum deposited small molecular materials which showed high structural orders in the solid state. The FET performance of solution-processed small molecular and polymer semiconductors remained generally poor.

An electrochemically polymerized thiophene was first used in OTFTs in mid-1980s, showing very low mobility of $10^{-5}\ cm^2 V s^{-1}$.[9] Shortly after, soluble regiorandom poly(3-alkylthiophenes) (**1a**), prepared via $FeCl_3$-mediated oxidative coupling, were utilized and again with low mobility. This was obviously due to lack of crystalline orders in amorphous thin films.[13] Other approaches using Langmuir–Blodgett films and mechanic stretch/alignment to enhance molecular ordering also failed to improve FET performance.[14,15]

With newly developed regioregular polymerization methods for polythiophenes,[16,17] regioregular head-to-tail poly(3-alkylthiophenes) **1b** (HT-P3AT), with high regioregularity ($\geq$95%), were successfully synthesized. Regioregular HT-P3ATs such as poly(3-hexylthiophene) HT-P3HT (**1b**, R = hexyl), exhibited solid-state properties (e.g., band gaps, crystallinity, and conductivity) significantly different from those of corresponding regiorandom counterparts. The high crystallinity of HT-P3HT semiconductor led to greatly improved FET performance in OTFTs.[18] The performance characteristics were however much superior when the devices were fabricated in inert atmospheres ($\mu \approx 0.1\ cm^2 V^{-1} s^{-1}$; $I_{on}/I_{off} \approx 10^6$)[19] than in ambient conditions ($\mu \approx 0.045\ cm^2 V^{-1} s^{-1}$; $I_{on}/I_{off} \approx 10$–$10^3$).[18] It was found that the polythiophene regioregularity had a decisive effect on the molecular ordering

and orientation of P3HT on the substrate, hence, a dramatic effect on mobility of OTFT devices.[20] X-ray diffraction (XRD) pattern of HT-P3HT with >95% regioregularity revealed that it formed lamellar π–π stacks and adopted an edge-on orientation with the lamellar stacks parallel to the substrate - a favourable molecular ordering conducive to charge carrier transport. On the other hand, HT-P3HT with ≈80% of head-to-tail regiochemistry showed a face-on orientation (lamellar stacks normal to the substrate), which accounted for the observed lower mobility ($2\times10^{-4}\,cm^2V^{-1}s^{-1}$).

The mobility of HT-P3HT varied greatly with its molecular weight and fabrication solvent.[21,22] High molecular weights provided higher mobility and this was attributed to formation of isotropic nodules as opposed to rod-like structures for lower molecular weight materials. The former afforded better interconnection between domains, thus reducing the barriers to interdomain carrier transport. The observation that higher boiling-point solvents generally gave higher mobility stemmed from the fact that these solvents had slower evaporation rates and thus provided longer times for the polythiophene molecules to self-organize.

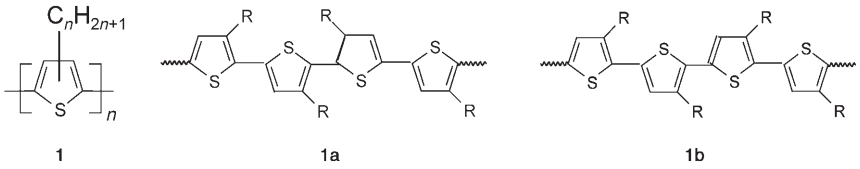

1 1a 1b

Copolymers of bithiophene and fluorene (e.g., **2**), which displayed liquid crystalline behaviours, yielded FET mobility of up to $0.02\,cm^2Vs^{-1}$ when properly annealed in its liquid crystalline phases.[23] These polymer semiconductors were relatively air stable, thus permitting device processing in ambient conditions. Regiorandom copolymers of 3-hexylthiophene and 3-methyl-thiophene, **3**, prepared from $FeCl_3$ coupling polymerization, yielded better mobility of $0.045\,cm^2V^{-1}s^{-1}$, albeit with a large positive turn-on voltage indicative of heavy oxygen doping.[24] An approach employing a soluble polymer precursor, and relied on its thermal conversion to insoluble poly(thienylene vinylene) semiconductor **4** was reported to give mobility of $0.22\,cm^2V^{-1}s^{-1}$,[25] but this high mobility has never been reproduced.[26]

Modified regioregular polythiophenes with different side-chains such as **5, 6**, and **7** had also been studied in OTFTs without improvement in FET performance.[27] These results clearly demonstrate the formidable challenge in fundamental design of high-mobility polymer semiconductors for OTFTs, which is additionally compounded by the needs to consider materials solution processability and sensitivity to ambient conditions.

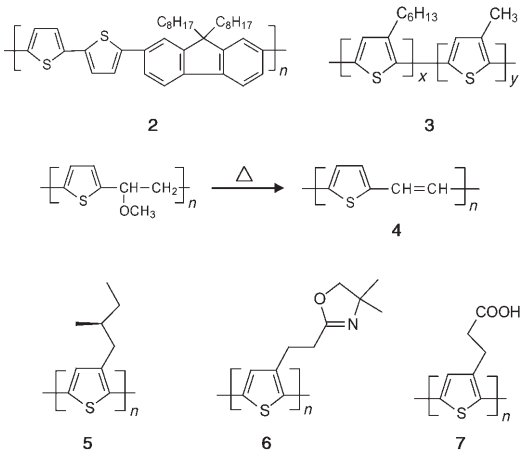

2 3 4 5 6 7

High-Mobility Thiophene Polymer Semiconductor Design

The poor FET performance of HT-P3HT fabricated under ambient conditions can be attributed to its sensitivity to atmospheric oxygen in the presence of ambient light. Two photoinduced phenomena of thiophene polymer semiconductors have been observed: i) photoinduced oxidative doping by oxygen, which occurs when the semiconductor material is exposed to ambient oxygen and light;[28] and ii) photo-oxidation or photobleaching which arises from the reaction of oxygen with the semiconductor molecules when exposed to ultra-violet radiation.[29,30] While photoinduced oxidative doping is thermally reversible, and accelerated under vacuum, photobleaching is irreversible.[30] Oxidative doping by oxygen, which leads to generation of free carriers in the semiconductor, is responsible for the occurrence of high off-current and thus a low I_{on}/I_{off} of transistor. Photobleaching, which destroys the conjugated structure of polythiophene semiconductor, results in a low FET mobility.[30] Nonetheless, regioregular polythiophenes are generally stable to oxygen in the dark, they are only susceptible to oxidative doping and photobleaching in air when exposed to ambient light.

The lamellar structural order of HT-P3HT in which all its thienylene moieties along the polymer backbone are held in coplanarity by intermolecular alkyl side-chain interaction,[31] results in a highly delocalized π-conjugated system. This represents an electron-rich structure which is highly susceptible to photobleaching by atmospheric oxygen in the presence of trace ultraviolet radiations. The highly extended π-conjugation of lamellar structural order also extends spectral absorption into visible region and brings about the propensity to photoinduced oxidative doping. Nevertheless, the fact that HT-P3HT was capable of achieving high mobility and current on/off ratio in OTFTs in an inert atmosphere or in

the dark demonstrated its excellent intrinsic FET properties. These results suggested that a plausible approach to a high-performance polymer semiconductor was possible if appropriate structural features could be incorporated into the polymer semiconductor structure to control its π-conjugation for air stability without compromising FET properties.[31] We believed that this could be accomplished with a specifically designed polythiophene system through deployment of the following design principles:[32–35] i) strategically distributed long alkyl side-chain substitution to provide solution processability and molecular self-assembly efficacy; and ii) proper control of π-conjugation to achieve a delicate balance between air stability and FET properties. The requirement for building stability against oxidative doping and photobleaching in a semiconductor structure without compromising its FET properties is perhaps most demanding in semiconductor development. Through structural studies, we found that simple torsional deviation of strategically placed conjugating moieties M from coplanarity along polymer backbone as described by structure **I** can be very effective in tuning π-conjugation of regioregular thiophene polymers for air stability and FET properties.

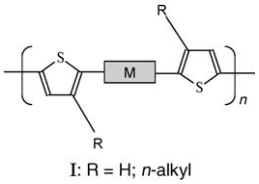

I: R = H; *n*-alkyl

Poly(dialkylterthiophene)s

Poly(3′,4′-dialkylterthiophene) **8** represents one of the simplest model polythiophene systems of **I** for the study of oxidative stability, self-assembly capability, and FET properties.[33] It was readily prepared from the corresponding monomer by $FeCl_3$-mediated oxidative coupling polymerization in good yields.[36] Polythiophene **8** with long alkyl side-chains

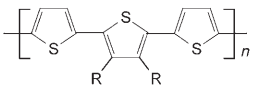

8

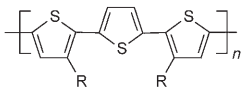

9

($R \geq C_6$) such as **8a** (R = *n*-decyl) displayed an ability to self-organize in the solid state when cast from solution, as reflected by a bathochromic shift in its UV/Vis absorption spectra from solution to thin film. The solution spectrum of **8a** also showed a progressive bathochromic shift with a concomitant appearance of a longer-wavelength shoulder with increased addition of a poor solvent such as methanol.[37] These spectral properties appeared to suggest formation of a co-facial π–π stacking order in the solid state. However, no lamellar structural order similar to that of HT-P3HT could be detected by X-ray diffraction (XRD) studies.

On the other hand, poly(3,3″-dialkylterthiophene) **9**, a regioisomer of **8** with a "spaced-out" alkyl side-chain distribution, exhibited a greater self-assembly ability.[34] While **8a** formed only a co-facial π–π stacking structure in thin films, **9a** (R = *n*-octyl) readily self-organized into a lamellar π-stacking structural order in the solid state when cast from solution, a result of extensive intermolecular side-chain interactions facilitated by the "spaced-out" side-chain distribution. The UV/Vis absorption spectrum of **9a** in solution showed a broad absorption at $\lambda_{max} \approx 470$ nm, typical of a twisted polythiophene conformation. However, the thin-film absorption of **9a** was sigificantly red shifted together with the appearance of vibronic splitting at $\lambda_{max} \approx 510$ (shoulder), 540, and 583 (shoulder) nm, indicative of a higher structural order than **8a** in the solid state. The thin-film spectral properties of **9a** were quite similar to those of HT-P3HT with a co-facial lamellar π-stacking structural order, in sharp contrast to those of **8a** which displayed indiscernible vibronic features. XRD pattern of a thin film of **9a** showed diffraction peaks at $2\theta = 5.8$ (100), 11.8 (200), and 17.8° (300), corresponding to an interlayer spacing of 15.1 Å. The transmission electron diffraction showed a diffraction corresponding to a co-facial π–π stacking distance of ≈3.9 Å. These results support a lamellar structural order of **9a** in the solid state.

OTFTs fabricated with **8a** and **9a** under ambient conditions afforded favorable FET characteristics which conformed to the metal oxide-semiconductor FET gradual channel model.[33,34] The extracted mobility from the saturated regime was $\approx 0.01\ cm^2 V^{-1} s^{-1}$ (on/off ratio of $\approx 10^5$) and $0.03\ cm^2 V^{-1} s^{-1}$ (on/off ratio $\approx 10^6$) respectively. While these FET results were quite similar to those of HT-P3HT devices fabricated under ambient conditions, the stabilities of **8a** and **9a** were significantly much better. Nonetheless, these FET performance characteristics were still short of our expectation. We envisioned that a lamellar π-stacking structural order of this type with a tighter packing would lead to significantly higher mobility, thus opening up opportunities for wider applications.

Poly(dialkylquarterthiophene)s

Regioregular poly(3,3‴-dialkyl-quaterthiophene) **10** (PQT) is a poly(dialkylquarterthiophene) system with two alky side-chains at C-3 and C-3‴ positions of its repeating units, thus, enabling an alternating *syn-trans* distribution of side-chains along polymer backbone in the stretched-out coplanar conformation. With appropriate alkyl side-chain substitution, PQT would be expected to exhibit excellent solution processability as well as self-assembly ability. Regioregular PQT has a repeating length of about 15.5 Å. Thus, the *d*-spacing of alkyl side-chains oriented in the same direction in the extended coplanar conformation of PQT is approximately 12 Å, since the side-chains are tilted at an angle of ≈50° against the backbone. This 12 Å spacing together with a sufficiently long alkyl side-chain would enable PQT to self-assemble more efficiently through intermolecular side-chain interdigitation. The result would be a strongly held lamellar structure, enabling a long-range lamellar π-stacking order in the solid state. Lamellar structures of this type have been observed in the oligomeric forms of PQT.[38] The presence of

unsubstituted thienylene moieties, which are expected to assume certain torsional deviations from coplanarity, would cut down on the π-conjugation to provide the needed air stability. PQT was prepared from the corresponding quarterthiophene monomer in good yields by $FeCl_3$-mediated oxidative coupling polymerization, and purified by extraction with appropriate solvents.[35] The thin-film absorption spectrum of PQT-12 (see Scheme 1, n = n-dodecyl) displayed significantly longer-wavelength absorptions with well-resolved vibronic splitting, even though its solution spectrum was quite similar to those of poly(terthiophene)s.

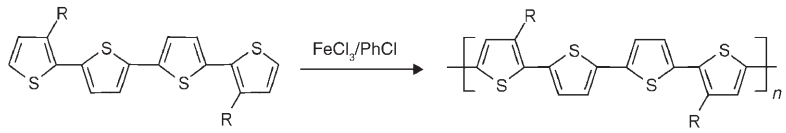

Scheme 1. Synthesis of PQT.

As expected, PQT-12 possessed an ionization potential which is ≈0.1 eV higher than that of HT-P3HT and a wider band gap, indicative of its greater stability against photoinduced oxidative interactions. Differential scanning calorimeter (DSC) thermogram of PQT-12 showed liquid crystalline characteristics with two endotherms at 120 and 140 °C, corresponding respectively to the crystalline-to-liquid crystalline and liquid crystalline-to-isotropic phase transitions.[35] The XRD pattern of a powdered sample of PQT-12 showed two diffraction peaks at $2\theta = 7.4$ and 21.5°, arising from the side-chain (d spacing, 12.0 Å) and π–π stacking (d spacing, 4.1 Å) orderings respectively. When the powdered sample was annealed at 120–140 °C, highly crystalline XRD patterns were observed, revealing a shortened interchain d spacing of 16.4 Å and a π–π stacking distance of 3.8 Å. An annealed thin film of PQT-12 on an OTS-8-modified silicon wafer substrate displayed XRD diffraction peaks at $2\theta = 5.1$ (100), 10.3 (200) and 15.4° (300), corresponding to an interlayer distance of 17.3 Å. Transmission electron diffraction analysis gave a π–π stacking distance of 3.7 Å. These results support formation of lamellar π–π stacking structures which were preferentially oriented with their lamellar (100) axes normal to the substrate. Thus it can be concluded that PQT-12 possessed an excellent ability to organize into highly ordered lamellar π–π stacking structures whose orientation could be manipulated through surface chemistry and alignment techniques. This was reminiscent of the self-assembly behaviours of regioregular poly(3-alkylthiophene)s.[23]

As a channel semiconductor in OTFTs fabricated under ambient conditions and annealed at 120–145 °C, PQT-12 exhibited excellent FET properties. The output characteristics showed no noticeable contact resistance, very good saturation behavior, and clear saturation currents which were quadratic to the gate bias (Figure 3). The device switched on nicely at around 0 V with a subthreshold swing of 1.5 V dec^{-1}. Extracted mobility of up to 0.2 cm^2 V^{-1} s^{-1} and on/off ratio of 10^6–10^8 were obtained. The ability to achieve high mobility and extremely high on/off ratio with the OTFT devices fabricated under ambient conditions affirmed the significantly greater environmental stability of PQT-12. In addition, the mobility values extracted from both the linear and saturated regimes were about the same, and no observable differences were noted with the top- and bottom-contact device configurations. Little or no hysteresis and bias stress effects were observed with these devices at and above room temperature. All these data suggest that PQT-12 was an excellent all-round semiconductor for OTFTs.

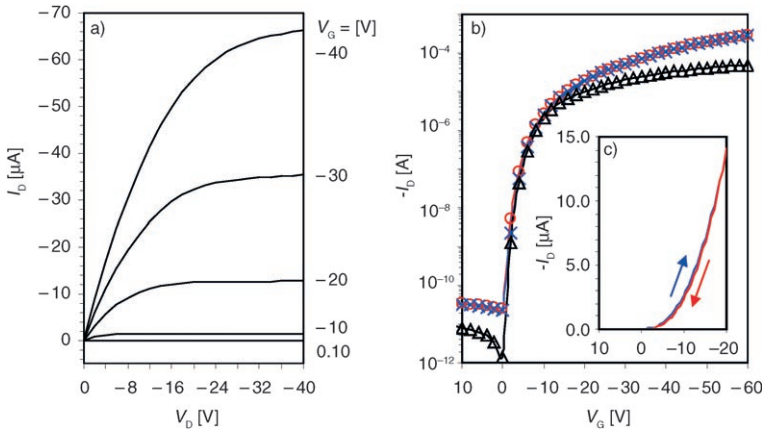

Figure 3. I/V characteristics of exemplary PQT-12 TFT device with 90-μm channel length and 5000-μm channel width: a) output curves at different gate voltages; b) two transfer curves in saturated regime scanned from positive to negative gate voltages (○ and ×, $VB_{DB} = -60$ V) and transfer curve at linear regime (△, $VB_{DB} = -6$ V); c, two transfer curves scanned in different directions between +10 V and −20 V (from ref. [35]).

As the surface chemistry of dielectric layer has great influence on molecular ordering of overlaying semiconductor and thus its FET properties, the effects of silane modification of dielectric surface on PQT-12 performance were carefully studied.[39] Different silane agents were used to modify SiO_2 surface in order to control the molecular ordering and orientation of PQT-2. The results showed that with silane modification, the OTFT devices exhibited dramatic improvement in mobility over those on bare SiO_2 dielectric by as much as two orders of magnitude. Among all the silane agents studied, OTS-8 and dodecyltrichlorosilane were

found to be most efficient for achieving optimal PQT-12 ordering for FET performance. This was attributable to a stronger interaction between comparable alkyl chain lengths of these silane agents with the dodecyl side-chains of PQT-12. Although X-ray diffraction did not reveal any noticeable differences in the PQT-12 films on various silane-treated SiO_2 surfaces, AFM measurements did show some different surface morphologies.[40]

Surprisingly, while the spin-coated PQT-12 semiconductor layers provided consistent FET results, significant variations in mobility and current on/off ratio of OTFTs were noted when inkjet printing was used in patterning PQT-12 semiconductor layers. The root cause of the discrepancy was traced to the tendency of PQT-12 solution to gel at low temperatures ($\geq 50\,^{\circ}C$) leading to non-uniformity in the inkjet printed PQT-12 layers and thus inconsistent FET performance. This gelling complication would be expected to present serious practical challenge to OTFT fabrication, and undermine a cost-effective manufacturing feasibility. Through our studies of solution behaviours of PQT, we had successfully developed a PQT-12 nanoparticle material to circumvent this difficulty.[41] PQT-12 nanoparticles, when dispersed in a suitable liquid medium, formed a stable nanoparticle ink which enabled printing of reproducible, functionally capable semiconductor layers for OTFTs.

The PQT-12 nanoparticle ink was successfully utilized in fabricating the semiconductor channels of active-matrix TFT array backplanes for flat-panel displays using inkjet printing technique.[42] Specifically, the nanoparticle ink was jetted into the TFT channels of a pre-patterned TFT array structure using a piezoelectric inkjet printer. The resulted OTFTs exhibited a FET mobility of 0.05–0.10 $cm^2 V^{-1} s^{-1}$, and a current on/off ratio of $\approx 10^6$ at $V_{SD} = -40$ V. The onset voltage was close to 0 V and the subthreshold slope was 75 $nF V dec^{-1} cm^{-1}$. The output characteristics showed good saturation with no signs of significant contact resistance. In addition, the OTFTs displayed a minimal gate bias stress effect. All these properties obtained for the inkjet-printed TFTs were very similar to those of spin-coated devices. A high yield of working OTFTs and uniformity in both the on- and off-current were also observed. A typical series of measurements gave an average mobility of 0.06 $cm^2 V^{-1} s^{-1}$, with standard deviation of 0.02 $cm^2 V^{-1} s^{-1}$. These results represent the state-of-the-art polymer OTFTs with higher average mobility than the pentacene-OTFTs from a solution processed precursor[43] recently used in prototyping electrophoretic display and RFID devices.

Poly(2,5-bis(2-thienyl)-thieno[3,2-*b*]thiophene)s

A simple approach to structurally optimizing polythiophene systems such as PQT to improve FET properties is to shorten the spacing between its pendant side-chains to strengthen intermolecular side-chain interdigitation. This could readily be accomplished through fusion of two adjacent thienylene moieties of PQT structure into thienothiophene to form poly(2,5-bis(2-thienyl)-thieno-thiophenes **11** and **12** as depicted in Figure 4. Poly(2,5-bis(3-dodecylthiophen-2-yl)-thieno[3,2-*b*]thiophene) **11a** (R = *n*-dodecyl) was reported to provide a FET mobility of 0.2–0.6 $cm^2 V^{-1} s^{-1}$ and a current on/off ratio of 10^6 when measured under a nitrogen atmosphere.[44] Latest studies provided a mobility of 0.3 $cm^2 V^{-1} s^{-1}$ even after annealing at 180 °C in a nitrogen glove box.[45]

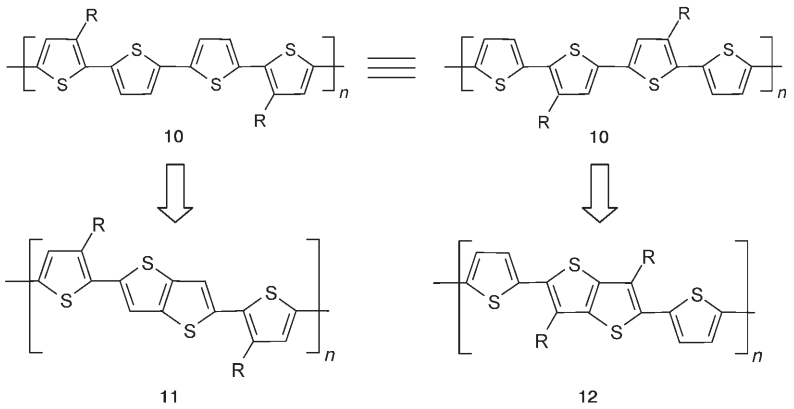

Figure 4. Fusion of two adjacent thienylene units in PQT to form poly(2,5-bis-(3-alkylthiophen-2-yl)-thieno-[3,2-*b*]thiophene **11** and poly(2,5-bis(2-thienyl)-3,6-dialkylthieno[3,2-*b*]thiophene **12**.

The other modified PQT with close side-chain spacing, poly(2,5-bis(2-thienyl)-3,6-dipentadecylthieno[3,2-*b*]thiophene) **12a** (PTAT-15, R = *n*-pentadecyl), also provided about the same FET mobility.[46] In dilute chlorobenzene solution, PTAT-15 showed a strong absorption with λ_{max} at 467 nm in its UV/Vis absorption spectrum, while its thin film (annealed at 150 °C) displayed absorption with λ_{max} at 496 nm, along with two shoulders at 460 and 530 nm. This small red-shift in absorption from solution to thin film ($\approx$30 nm) was in sharp contrast to those of regioregular polythiophenes such as HT-P3HT ($\approx$100 nm) and PQT-12 ($\approx$75 nm), suggesting that PTAT-15 might have assumed a conformation with twisted thienylene units in the solid state. The HOMO level of PTAT-15, as determined by cyclic voltammetry, was 5.23 eV from vacuum, which was much lower than those of most regioregular polythiophenes [e.g., HT-P3HT $\approx$5.0 eV; PQT-12 $\approx$5.1 eV; and poly(2,5-bis(3-dodecylthiophen-2-yl)thieno[3,2-*b*]thiophene) $\approx$5.1 eV.[44] The low-lying HOMO together with a large band gap was expected to confer on PTAT-15 greater air stability. DSC analysis of PTAT-15 showed only a sharp endotherm at 148 °C on heating, arising from backbone melting. This was much

lower than that of poly(2,5-bis(3-alkylthiophen-2-yl)thieno-[3,2-*b*]-thiophene) at 244–251 °C.[44] This disparity arose from the alkyl side-chain placement on the thieno[3,2-*b*]thiophene instead of thienylene moieties in PTAT-15 (Scheme 2), thus allowing its thienylene units substantial torsional deviations from coplanarity with the molecular plane in the solid state. This gave rise to a much lower backbone melting temperature than **11a**, thus enabling PTAT-15 to be annealed at ≈150 °C—a temperature which is compatible with the dimensional stability and structural integrity of commercial plastic substrates. The OTFT devices incorporating PTAT-15 semiconductor annealed at ≈150 °C showed excellent FET characteristics with the mobility up to 0.25 $cm^2 V^{-1} s^{-1}$, a current on/off ratio of 10^7, a near-zero turn-on voltage, a small threshold voltage of −8 V, and a sub-threshold slope of ≈1.5–2 $V dec^{-1}$.

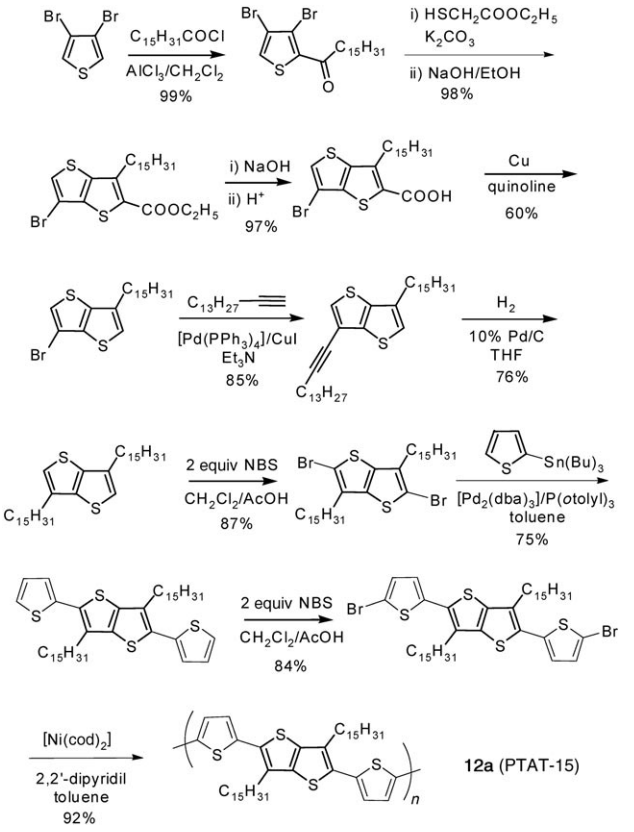

Scheme 2. Synthesis of poly(2,5-bis(2-thienyl)-3,6-dipentadecylthieno[3,2-*b*]thiophene, PTAT-15.

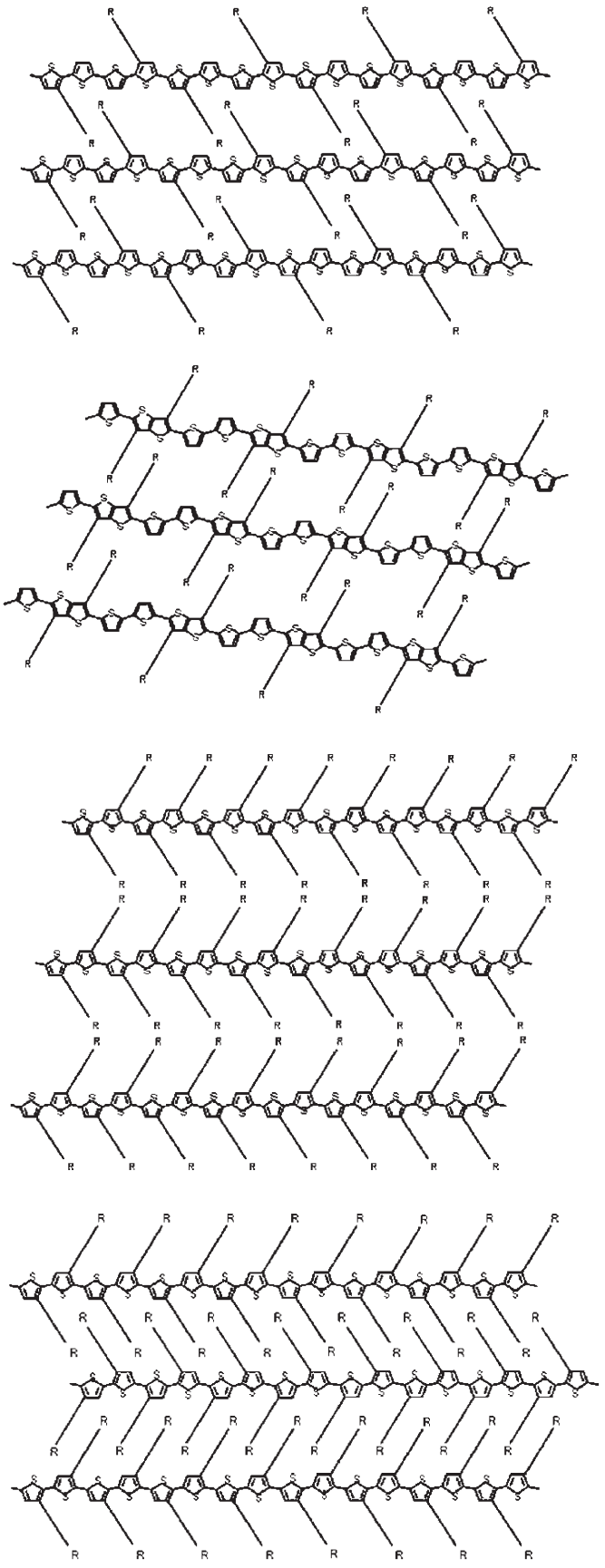

Figure 5. Intermolecular interactions of pendant alkyl side-chains in lamellar structures of regioregular polythiophenes: a) side-chain interdigitation in PQT-12; b) side-chain interdigitation in PTAT-15; c) end-to-end side-chain interaction in HT-P3HT; and d) side-chain interdigitation in HT- P3HT.

Poly(benzodithiophene)s and Copolymers

As one of the primary driving forces behind OTFTs is low cost, any materials characteristics which critically impact the economy of manufacturing would require serious consideration. High throughput is central to lowering manufacturing cost, thus roll-to-roll processes are generally considered to be paramount for driving manufacturing productivity.

Unfortunately, most if not all efficient organic semiconductors such as PQT and poly(bis(2-thienyl)-thieno[3,2-*b*]thiophene)s **11a** and **12a**, require further conditioning or annealing after semiconductor deposition to achieve high mobility. The annealing steps are time consuming and often carried out at relatively high temperatures (>100 °C) either in vacuum or an inert atmosphere. Such post-deposition annealing steps are not compatible with the high speeds of roll-to-roll processes needed to deliver the low-cost economic advantage. Accordingly, to realize low-cost OTFTs, the annealing step would have to be eliminated.

Regioregular thiophene polymers such as PQT-12 and PTAT-15 with well-spaced alkyl side-chain distributions exhibited backbone melting at relatively high temperatures (≈140–150 °C) They self-organized into highly crystalline lamellar π–π stacking structural orders via intermolecular side-chain interdigitation (Figure 5a and b) upon deposition from solution when heated to backbone melting temperatures followed by slow cooling. Similarly, for poly(2,5-bis(3-dodecylthiophen-2-yl)thieno[3,2-*b*]thiophene), crystalline state was induced by heating to its backbone melting temperature of about 244–251 °C followed by cooling. However, HT-P3HT self-assembled readily at room temperature into a highly crystalline state when deposited from solution without additional thermal assistance.[20,31] This was primarily made possible by the sterically crowded side-chain distribution along the backbone of HT-P3HT, which rendered ordering via intermolecular side-chain end-to-end interaction energetically favorable (Figure 5c). On the other hand, the steric congestion of pendant side-chains in HT-P3HT also made intermolecular side-chain interdigitation (Figure 5d) energetically demanding.

Accordingly, we envisaged that a plausible approach to achieving low-temperature structural ordering in a polymer semiconductor was to build a regioregular system with a crowded pendant side-chain distribution along the backbone. Such a system would be expected to self-assemble into crystalline states by adopting an end-to-end side-chain interaction much like that in HT-P3HT. Benzodithiophene nucleus **13** was selected for the verification of this hypothesis on the following considerations: i) it permitted building three different fundamental structural designs **14** ($R \geq C_6$), **15** ($R \geq C_6$) and **16** ($R \geq C_6$) to study three unique steric environments of pendant side-chain distributions on structural

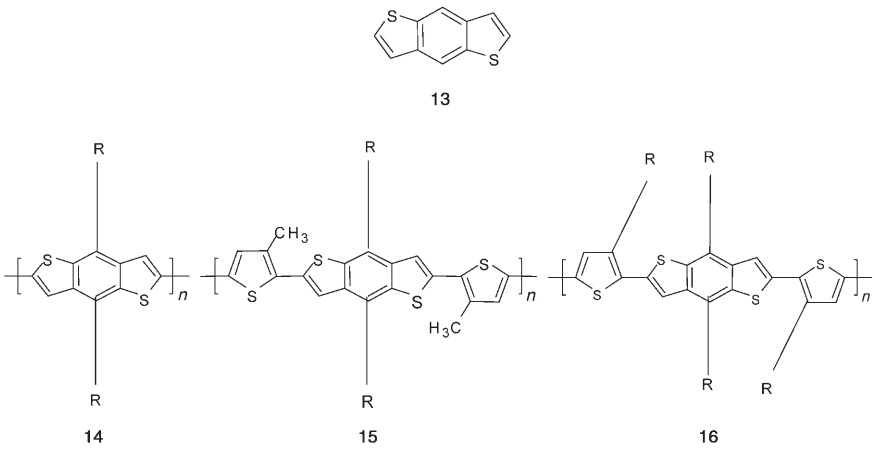

ordering, and thus FET characteristics; and ii) it was thermally and oxidatively very stable, and its relatively large and planar molecular structure would help promote cofacial π–π stacking which is beneficial to charge transport. As can be noted, **16** possessed a crowded pendant alkyl side-chain distribution along the backbone, and would behave much like HT-P3HT in self-organization through end-to-end side-chain ordering. On the other extreme, **15** with a small methyl substituent and a long alkyl side-chain, provided a well-spaced alkyl side-chain distribution and would adopt an interdigitation ordering model, while **14** was somewhere in between in terms of steric congestion and might adopt interdigitation ordering when thermally driven. A general synthetic route to these polymers is described in Scheme 3.[48–50]

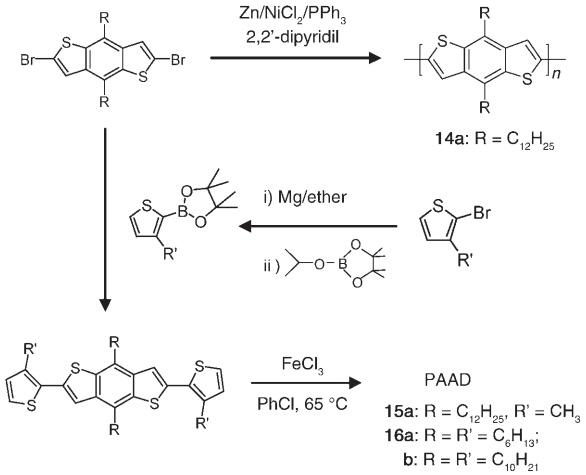

Scheme 3. Synthesis of poly(benzodithiophene)s and copolymers.

Depicted in Figure 6 are the single crystal structures of monomers of the three polymers, demonstrating side-chain interdigitation in the monomers of **14** and **15** while an end-to-end arrangement of side-chains in **16**. These two distinct modes of molecular ordering were also reflected in the structural organizations of the corresponding polymers **14**–**16** as schematic represented in Figure 7 through XRD analysis.[48–50]

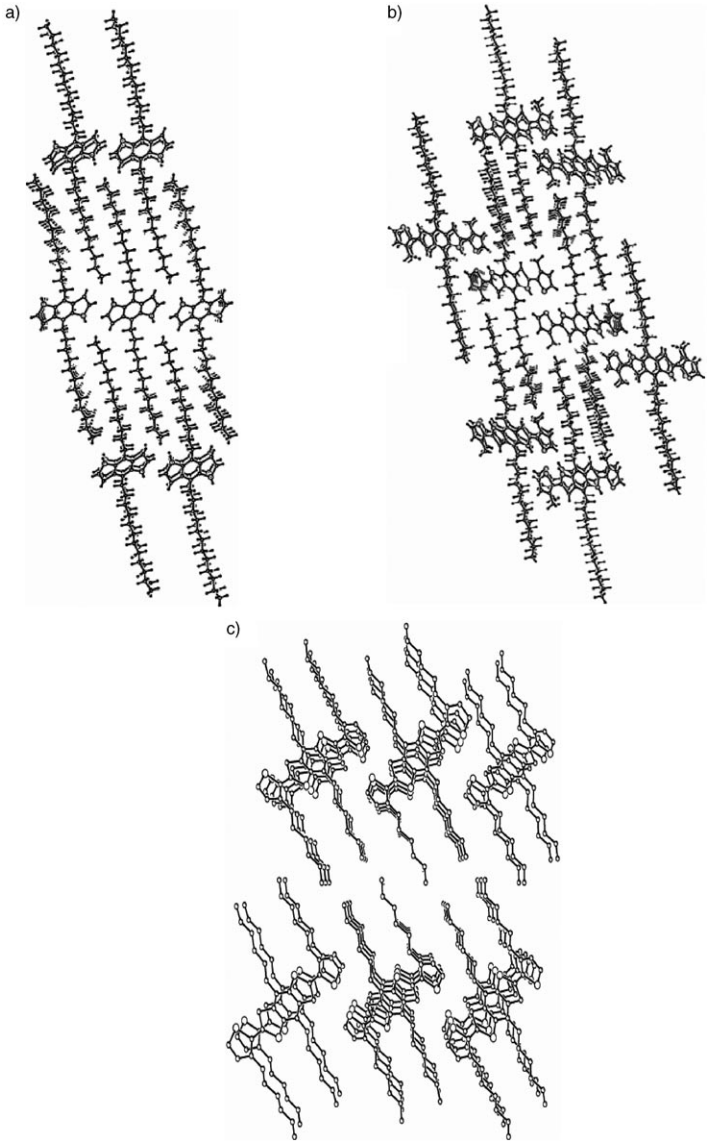

Figure 6. Single crystal structures of a) 4,8-didodecylbenzo[1,2-*b*:4,5-*b*′]dithiophene (monomer of **14**); b) 4,8-didodecyl-2,6-bis(3-methylthiophen-2-yl)benzo[1,2-*b*:4,5-*b*′]dithiophene (monomer of **15**); and c) 4,8-dihexyl-2,6-bis(3-hexylthiophen-2-yl)benzo[1,2-*b*:4,5-*b*′]dithiophene (monomer of **16**) showing different intermolecular side-chain orderings.

DSC analysis revealed that **14** had two melting temperatures at ≈140 and ≈280 °C corresponding respectively to side-chain and backbone melting.[48] On the other hand, **15** displayed no thermal transitions up to 300 °C on both heating and cooling.[49] Obviously, the relatively small methyl substituents and the large spacing between the dodecyl side-chains in **15** did not present any steric barriers to the otherwise energetically demanding interdigitation process. However, when both the alkyl substituents were the same and sufficiently long such as hexyl in **16a** (R = R′ = hexyl; PAAD-6), interdigitation was prevented, and ordering occurred via end-to-end side-chain interaction. **16a** displayed only one thermal transition at ≈395 °C in its DSC thermogram.[50]

Detailed characterization by two-dimensional grazing-incidence X-ray-diffraction (GIXRD, incident X-ray angle of 2.5°) analysis showed that a spin-cast thin film of **16a** on an OTS-8-modified silicon wafer substrate exhibited only a strong primary diffraction pattern (100) at $2\theta = 5.6°$ (Figure 8c), demonstrating a well-organized lamellar structure which was oriented normal to the substrate.[50] The (010) diffraction from π–π stacking was not observed due to blockage by the substrate. The highly ordered structure of **16a** was unambiguously demonstrated through two-dimensional transmission X-ray diffraction of a stack of thin films of **16a** as schematically depicted in Figure 8b. Figure 8d is the diffraction pattern obtained when the incident X-ray was normal to the film stack, showing both a strong π–π stacking (010) at $2\theta = 22.6°$ (d spacing, 3.9 Å) and a weak interlayer (100) diffractions. Strong (100), (200), (300) and (010) diffraction patterns were detected when the incident X-ray was parallel to the film stack (Figure 8e), showing the π–π stacking and interlayer diffraction patterns which were normal to each other. The highly organized nature of **16** in a solution processed thin film was manifested by the formation of extraordinarily large domains of ≈1 μm in width and >1 μm in length (Figure 9), in comparison to those of other polythiophenes, as visualized in the AFM images.

TFT studies using these polymers as channel semiconductors demonstrated FET properties which were in excellent agreement with the expectations based on structural and ordering considerations.[48–50] Semiconductor **14** gave a low FET mobility of ≈0.001 $cm^2 V^{-1} s^{-1}$ ($I_{on}/I_{off} \approx 10^5$). The mobility was improved by one order of magnitude to ≈0.012 $cm^2 V^{-1} s^{-1}$ after annealing at 140 °C, demonstrating achievement of a higher structural ordering following thermal treatment. On the other hand, **15** provided good mobility of 0.10–0.15 $cm^2 V^{-1} s^{-1}$ ($I_{on}/I_{off} \approx 10^6$) without thermal annealing. Thermal annealing did not lead to improvement in mobility, in agreement with the XRD observation that **15** had already achieved optimum structural ordering at room temperature. In line with the ability to achieve high crystalline orders in solution-cast thin films via end-to-end side-chain interaction, both **16a** and **16b** exhibited excellent FET characteristics as channel semiconductors in OTFTs. Specifically, the output behaviors followed closely the metal oxide-semiconductor FET gradual channel model, showing very good saturation with no observable contact resistance. The transfer characteristics of **16a** displayed a near-zero turn-on voltage, a small threshold voltage of −5.9 V, and a subthreshold slope of ≈2 $V.dec^{-1}$. The extracted saturation mobility

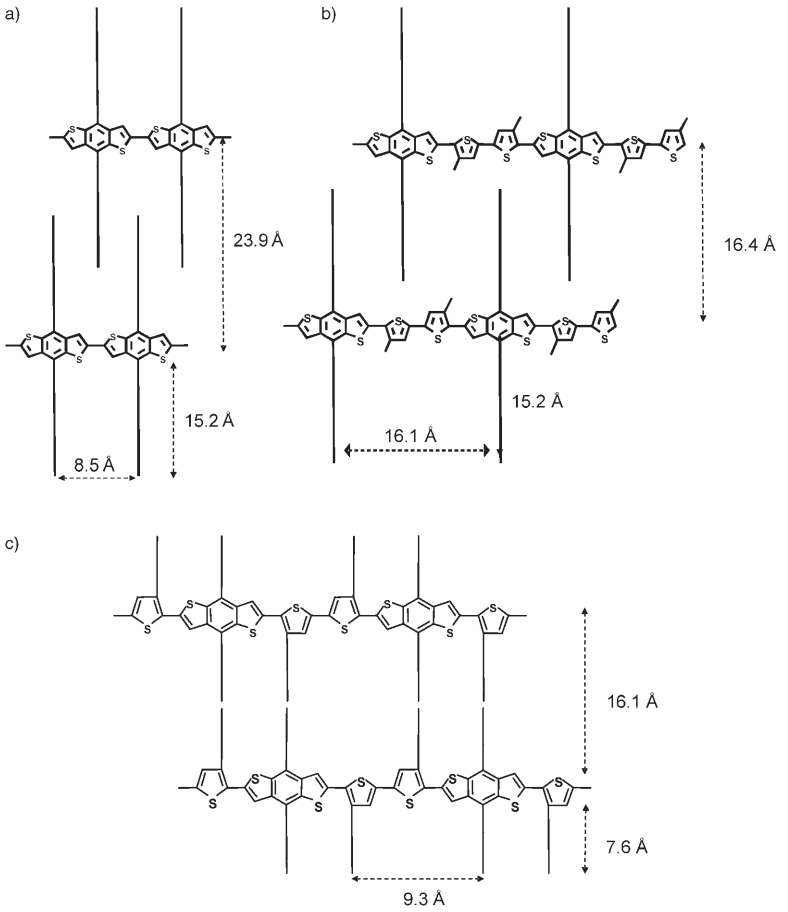

Figure 7. Schematic representations of structural orderings in solution cast thin films of thiophene polymers as deduced from XRD data: a) side-chain interdigitation of poly(4,8-didodecylbenzo[1,2-*b*:4,5-*b*′]dithiophene); b) side-chain interdigitation of poly(4,8-didodecyl-2,6-bis(3-methylthiophen-2-yl)benzo[1,2-*b*:4,5-*b*′]dithiophene); and c) end-to-end side-chain interaction of poly(4,8-dihexyl-2,6-bis(3-hexylthiophen-2-yl)benzo[1,2-*b*:4,5-*b*′]dithiophene).

was up to $\approx 0.25\ cm^2 V^{-1} s^{-1}$ ($I_{on}/I_{off} \approx 10^5$–$10^6$) without requiring post-deposition annealing. Devices with **16b** showed even higher mobility of up to $\approx 0.4\ cm^2 V^{-1} s^{-1}$ with $I_{on}/I_{off} \approx 10^6$. Annealing at temperatures up to ≈150 °C did not lead to improved FET performance as **16** was sterically too congested to undergo interdigitation to achieve a tighter structural order. This was in sharp contrast to the behaviors of most polymer thin-film semiconductors such as PQT and its analogues. The TFT devices of **16** also exhibited relatively stable performance over time as no significant degradation in mobility after standing over an extended period of time. Since post-deposition annealing is not necessary, **16** thus represents the current benchmark high-performance polymer semiconductor which may potentially enable high-speed roll-to-roll mass manufacturing of low-cost OTFT arrays/circuits.

Conclusion and Outlook

We have demonstrated that for polymer semiconductors, particularly thiophene-based polymers for FET applications, stability against photoinduced oxidative doping and to some extent photobleaching can be achieved through incorporation of appropriate structural moieties into the polymer backbone to control its π-conjugation. This would result in lowering its HOMO to suppress vulnerability to oxidation. Consideration should also be given in establishing sufficient π-conjugation in a delicate balance to achieve both FET mobility and ambient stability. PQT-12 and PTAT-15 are two good examples wherein both reasonable ambient stability and FET mobility are simultaneously accomplished.

Nonetheless, these semiconductor polymers still require post-deposition thermal annealing to achieve optimum structural ordering via side-chain interdigitation—a process that is tedious and time-consuming and is not amenable to high-speed roll-to-roll mass manufacturing processes for low-cost production. This difficulty has been circumvented with a semiconductor polymer design that mimics the sterically crowded side-chain distribution of HT-P3HT in driving the semiconductor molecules to order via end-to-end side-chain interaction—a process that appears to be readily achieved at room temperature as demonstrated by HT-P3HT. For a high-mobility polymer semiconductor design, the large

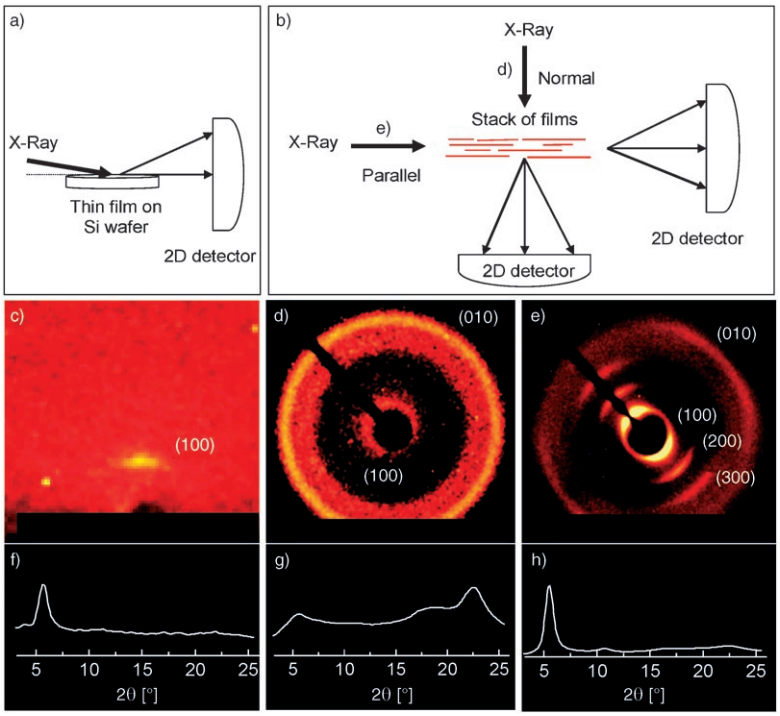

Figure 8. Schematic illustrations of a) 2D GIXRD measurement (incident X-ray angle at 2.5°) of a thin film of **16a** and b) 2D transmission XRD measurement of a stack of thin films of **16a**; c) 2D GIXRD images of a thin film of **16a**; 2D transmission XRD images obtained with the incident X-ray normal (d) and parallel (e) to the film stack of **16a**; f), g) and h) are respective XRD diffractograms of pattern intensities of c), d) and e) [obtained by integration of χ (0–360°) with GADDS software] (from ref. [50]).

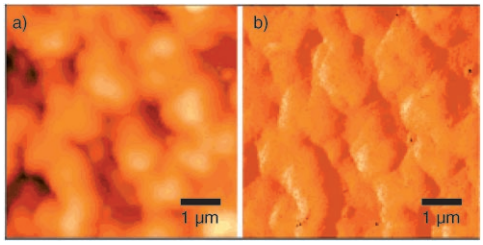

Figure 9. AFM images of a representative thin film of **16**: a) topography image; b) phase image showing large domains of 1 μm in width and >1μm in length (from ref. [50]).

and relatively planar benzodithiophene repeating unit which is efficient in promoting co-facial π–π stacking has proven to be particularly effective. This would give rise to an extended structural ordering in the form of lamellar π–π stacks which are conducive to charge transport by hopping. Polymer **16** (PAAD) represents such as a system with demonstrated ability to achieve high crystallinity via end-to-end side-chain ordering when cast from solution on an appropriate substrate without the need for thermal annealing. OTFTs using **16b** (PAAD-10) has shown excellent FET properties with mobility up to $\approx 0.4\ cm^2 V^{-1} s^{-1}$ and current on/off ratio of 10^6, together with other highly desirable FET characteristics. While the current mobility may not be high enough for application in backplane electronics for very large displays, it is certainly more than sufficient for use in e-paper and signage, sensing electronics and RFID tags using small channel TFTs. The fact that **16** does not require post-deposition thermal annealing is particularly advantageous as this would render high-throughput roll-to-roll mass manufacturing processes possible. It is our belief that continued progress in semiconductor design will be made in the near future in driving mobility up to a level suitable for a wider spectrum of high-value applications including backplanes for driving large flat-panel displays.

Semiconductor is only one of many critical component materials for OTFT arrays/circuits. For low-cost applications, particularly for use in flexible electronic devices, other solution processable or printable components such as gate dielectric, electrical conductor, and protective encapsulation materials are also required. It is encouraging to witness that these essential materials have in recent years been receiving growing research attention, and that significant advances have also been made in these areas.[51–56]

[1] *Organic Electronics: Materials, Manufacturing, and Applications* (Ed.: H. Klauk), Wiley-VCH, Weinheim (Germany), **2006**.
[2] *Flexible flat panel display* (Ed.: G. P. Crawford), Wiley, New York, **2005**.
[3] *Printed organic and molecular electronics* (Eds.: D. Gamota, P. Brazis, K. Kalyanasumdaram, J. Zhang), Kluwer Academic, Boston, **2004**.
[4] J. Veres, S. D. Ogier, S. W. Leeming, D. C. Cupertino, S. M. Khaffaf, *Adv. Funct. Mater.* **2003**, *13*, 199–204.
[5] Y. Li, Y. Wu, B. S. Ong, *Macromolecules* **2006**, *39*, 6521–6527.

[6] W. Porzio, S. Destri, M. Pasini, A. Bolognesi, A. Angiulli, P. Di Gianvincenzo, D. Natali, M. Sampietro, M. Caironi, L. Fumagalli, S. Ferrari, E. Peron, F. Perissinotti, *Mater. Sci. Eng. C* **2006**, *26*, 996–1001.
[7] G. H. Heilmeier, L. A. Zanoni, *J. Phys. Chem. Solids* **1964**, *25*, 603–611.
[8] F. Ebisawa, T. Kurokawa, S. Nara, *J. Appl. Phys.* **1983**, *54*, 3255–3259.
[9] A. Tsumura, H. Koezuka, T. Ando, *Appl. Phys. Lett.* **1986**, *49*, 1210–1212.
[10] G. Horowitz, D. Fichou, X. Peng, Z. Xu, F. Garnier, *Solid State Commun.* **1989**, *72*, 385–388.
[11] T. Yamamoto, K. Takimiya, *J. Am. Chem. Soc.* **2006**, *128*, 12604–12605.
[12] T. W. Kelley, L. D. Boardman, T. D. Dunbar, D. V. Muyres, M. J. Pellerite, T. P. Smith, *J. Phys. Chem. B* **2003**, *107*, 5877–5881.
[13] A. Assadi, C. Svensson, M. Willander, O. Inganas, *Appl. Phys. Lett.* **1988**, *53*, 195–197.
[14] J. Paloheimo, P. Kuivalainen, H. Stubb, E. Vuorimaa, P. Yli-Lahti, *Appl. Phys. Lett.* **1990**, *56*, 1157–1159.
[15] S. Nagamatsu, W. Takashima, K. Kaneto, Y. Yoshida, N. Tanigaki, K. Yase, *Appl. Phys. Lett.* **2004**, *84*, 4608–4610.
[16] R. D. McCullough, S. Tristram-Nagle, S. P. Williams, R. D. Lowe, M. Jayaraman, *J. Am. Chem. Soc.* **1993**, *115*, 4910–4911.
[17] T. A. Chen, X. Wu, R. D. Rieke, *J. Am. Chem. Soc.* **1995**, *117*, 233–244.
[18] Z. Bao, A. Dodabalapur, A. Lovinger, *Appl. Phys. Lett.* **1996**, *69*, 4108–4110.
[19] H. Sirringhaus, N. Tessler, R. H. Friend, *Science* **1998**, *280*, 1741–1743.
[20] H. Sirringhaus, P. J. Brown, R. H. Friend, M. M. Nielen, K. Bechgaard, B. M. W. Langeveld-Voss, A. J. H. Spiering, R. A. J. Janssen, E. W. Meijer, P. Herwig, D. M. de Leeuw, *Nature* **1999**, *401*, 685–688.
[21] R. J. Kline, M. D. McGehee, E. N. Kadnikova, J. S. Liu, J. M. Frechet, *Adv. Mater.* **2003**, *15*, 1519–1522.
[22] J.-F. Chang, B. Sun, D. W. Breiby, M. M. Nielsen, T. I. Solling, M. Giles, I. McCulloch, H. Sirringhaus, *Chem. Mater.* **2004**, *16*, 4772–4776.
[23] H. Sirringhaus, R. J. Wilson, R. H. Friend, M. Inbasekaran, W. Wu, E. P. Woo, M. Grell, D. D. C. Bradley, *Appl. Phys. Lett.* **2000**, *77*, 406–408.
[24] J. Wang, Y. Y. Lin, W. Qian, T. N. Jackson, *MRS Fall Meeting Digest* **1998**, 372.
[25] H. Fuchigami, A. Tsumura, H. Koezuka, *Appl. Phys. Lett.* **1993**, *63*, 1372–1374.
[26] H. E. A. Huitema, G. H. Gelinck, J. B. P. H. van der Putter, K. E. Kujik, C. M. Hart, E. Cantatore, P. T. Herwig, A. J. J. M. van Breeman, D. M. de Leeuw, *Nature* **2001**, *414*, 599.
[27] Z. Bao, A. J. Lovinger, *Chem. Mater.* **1999**, *11*, 2607–2612.
[28] B. A. Mattis, P. C. Chang, V. Subramanian, Synth. Met. **2006**, *156*, 1241–1248.
[29] M. S. A. Abdou, F. P. Orfino, Y. Son, S. Holdcroft, *J. Am. Chem. Soc.* **1997**, *119*, 4518–4524.
[30] Y. Wu, B. S. Ong, unpublished results.
[31] T. Yamamoto, D. Komarudin, M. Arai, B.-L. Lee, H. Suganuma, N. Asakawa, Y. Inoue, K. Kubota, S. Sasaki, T. Fukuda, H. Matsuda, *J. Am. Chem. Soc.* **1998**, *120*, 2047–2058.
[32] B. S. Ong, Y. Wu, P. Liu, S. Gardner, *Polym. Prep.* **2003**, *44*, 321–322.
[33] B. S. Ong, Y. Wu, L. Jiang, P. Liu, K. Murti, *Synth. Met.* **2004**, *142*, 49–52.
[34] Y. Wu, P. Liu, S. Gardner, B. S. Ong, *Chem. Mater.* **2005**, *17*, 221–223.
[35] B. S. Ong, Y. Wu, P. Liu, S. Gardner, *J. Am. Chem. Soc.* **2004**, *126*, 3378–3379.
[36] C. Wang, M. E. Benz, E. LeGoff, J. L. Schindler, J. Allbritton-Thomas, C. R. Kannewurf, M. G. Kanatzidis, *Chem. Mater.* **1994**, *6*, 401–411.
[37] B. S. Ong, Y. Wu, P. Liu, *IEEE Transaction* **2005**, *93*, 1412–1419.
[38] P. Bäuerle, T. Fischer, B. Bidlingmeier, A. Stabel, J. P. Rabe, *Angew. Chem.* **1995**, *107*, 335–339; *Angew. Chem. Int. Ed. Engl.* **1995**, *34*, 303–307.
[39] Y. Wu, P. Liu, B. S. Ong, T. Srikumar, N. Zhao, G. Botton, S. Zhu, *Appl. Phys. Lett.* **2005**, *86*, 142102–142102–3.
[40] N. Zhao, G. Botton, S. Zhu, A. Duft, B. Ong, Y. Wu, P. Liu, *Macromolecules*, **2004**, *37*, 8307–8312.
[41] B. S. Ong, Y. Wu, P. Liu, S. Gardner, *Adv. Mater.* **2005**, *17*, 1141–1144.
[42] A. C. Arias, S. E. Ready, R. Lujan, W. S. Wong, K. E. Paul, A. Salleo, M. L. Chabinyc, R. B. Apte, R. A. Street, Y. Wu, P. Liu, B. Ong, *Appl. Phys. Lett.* **2004**, *85*, 3304–3306.
[43] G. H. Gelinck, H. Edzer, A. Huitema, E. van Veenendaal, E. Cantatore, L. Schrijnemakers, J. B. P. H. van der Putten, T. C. T. Geuns, M. Beenhakkers, J. B. Giesbers, B. Huisman, E. J. Meijer, E. M. Benito, F. J. Touwslager, A. W. Marsman, B. J. E. van Rens, D. M. de Leeuw, *Nat. Mater.* **2004**, *3*, 106–110.
[44] I. McCulloch, M. Heeney, C. Bailey, K. Genevicius, I. Macdonald, M. Shkunov, D. Sparrowe, S. Tierney, R. Wagner, W. M. Zhang, M. L. Chabinyc, R. J. Kline, M. D. McGehee, M. F. Toney, *Nat. Mater.* **2006**, *5*, 328–333.
[45] L. A. Lucas, D. M. DeLongchamp, B. M. Vogel, E. K. Lin, M. J. Fasolka, D. A. Fischer, I. McCulloch, M. Heeney, G. E. Jabbour, *Appl. Phys. Lett.* **2007**, *90*, 012112–012113.
[46] Y. Li, Y. Wu, P. Liu, M. Birau, H. Pan, B. S. Ong, *Adv. Mater.* **2006**, *18*, 3029–3032.
[47] A. S. Dhoot, J. D. Yuen, M. Heeney, I. McCulloch, D. Moses, A. J. Heeger, *Proc. Natl. Acad. Sci.* **2006**, *103*, 11834–11837.
[48] H. Pan, Y. Li, Y. Wu, P. Liu, B. S. Ong, S. Zhu, G. Xu, *Chem. Mater.* **2006**, *18*, 3237–3241.
[49] H. Pan, Y. Wu, Y. Li, P. Liu, B. S. Ong, S. Zhu, G. Xu, *Adv. Funct. Mater.* **2007**, *17*, 3574–3579.
[50] H. Pan, Y. Li, Y. Wu, P. Liu, B. S. Ong, S. Zhu, G. Xu, *J. Am. Chem. Soc.* **2007**, *129*, 4112–4113.
[51] P. Liu, Y. Wu, Y. Li, B. S. Ong, S. Zhu, *J. Am. Chem. Soc.* **2006**, *128*, 4554–4555.
[52] J. Veres, S. Ogier, G. Lloyd, *Chem. Mater.* **2004**, *16*, 4543–4555.
[53] A. Facchetti, M.-H. Yoon, T. J. Marks, *Adv. Mater.* **2005**, *17*, 1705–1725.
[54] Y. Wu, Y. Li, B. S. Ong, P. Liu, S. Gardner, B. Chiang, *Adv. Mater.* **2005**, *17*, 184–187.
[55] Y. Li, Y. Wu, B. S. Ong, *J. Am. Chem. Soc.* **2005**, *127*, 3266–3267.
[56] Y. Wu, Y. Li, B. S. Ong, *J. Am. Chem. Soc.* **2007**, *129*, 1862–1863.

Published online: March 25, 2008

